ADVANCED MATERIALS TECHNOLOGIES
www.advmattechnol.de

Electrohydrodynamic Jet Printing of One-Dimensional Photonic Crystals: Part I—An Empirical Model for Multi-Material Multi-Layer Fabrication

*Zahra Afkhami, Brian Iezzi, David Hoelzle, Max Shtein, and Kira Barton**

Electrohydrodynamic jet (e-jet) printing is a high-resolution additive manufacturing technique that holds promise for the fabrication of customized micro-devices. In this companion paper set, e-jet printing is investigated for its capability in depositing multilayer thin-films with microscale spatial resolution and nanoscale thickness resolution to create arrays of 1D photonic crystals (1DPC). In this paper, an empirical model for the deposition process is developed, relating process and material parameters to the thickness and uniformity of the patterns. Standard macroscale measurements of solid surface energy and liquid surface tension are used in conjunction with microscale contact angle measurements to understand the length scale dependence of material properties and their impact on droplet merger into uniform microscale thin-films. The model is validated with several photopolymer inks, a subset of which is used to create pixelated, multilayer arrays of 1DPCs with uniformity and resolution approaching standards in the optics manufacturing industry. It is found that the printed film topography at the microscale can be predicted based on the surface energetics at the microscale. Due to the flexibility in design provided by the e-jet process, these findings can be generalized for fabricating additional multimaterial, multilayer micro- and nanostructures with applications beyond the field of optics.

There has been a growing interest in the past decade in the fabrication of high-resolution, thin-film devices such as optical sensors,[1–3] flexible electronics,[4] memristor devices,[5] photonic crystals,[6] organic lasing cavities,[7] and transistors.[8,9] To realize high-performance, thin-film devices, the manufacturing process requires deposition of consistent, uniform layers with a repeatable thickness distribution across multiple material classes. Different manufacturing methods such as spin or dip coating,[10] lithography,[11] doctor blading,[12] chemical vapor deposition,[13] and others have been used to fabricate thin-film devices. However, most of these methods are limited by substrate planarity, high temperatures, harsh chemistries, or the dissolution of previous layers by non-orthogonal solvents.[14] Furthermore, in certain situations, it is desirable to deposit a customized pattern or to selectively place components on an existing device structure without disturbing it.

To address the challenges noted above, we examine an additive manufacturing (AM) approach and use it to realize vertically stacked, thin-film devices using multiple materials. AM technology in principle enables material deposition on nonplanar surfaces, by direct addition of material on existing topographies, without requiring cleanroom facilities and the use of masking steps more commonly used with lithography, and less material waste. Inkjet printing has been studied extensively for the creation of multimaterial, thin-film devices with demonstrated transistors[15–17] and optical sensors.[18] The thermal or piezo-driven excitation[19] used to deposit materials in a liquid phase in inkjet printing limits the achievable spatial resolution to larger than 20 μm. Furthermore, high viscosity inks (>50 cP) necessary for certain applications cannot be printed using inkjet technology.[20]

Electrohydrodynamic jet (e-jet) printing is a solution-based fabrication technique enabling thin-film fabrication and patterning without the planarity restrictions of lithography and other subtractive processes. Compared to inkjet technology, e-jet printing has a much higher spatial resolution (0.05–30 μm), comparable to the resolution of lithographic processes,[20,21] while also providing a high degree of freedom in creating customized patterns. Complex structures can be fabricated with high controllability and precision in desired locations from the micro- to nanoscale. E-jet is also capable of depositing a wide range of fluid viscosities from 10^0–10^5 cP, several orders of magnitude larger than that of inkjet printing.[19] This further enables

Z. Afkhami, Prof. K. Barton
Department of Mechanical Engineering
University of Michigan
Ann Arbor, MI 48109, USA
E-mail: bartonkl@umich.edu
B. Iezzi, Prof. M. Shtein
Department of Materials Science and Engineering
University of Michigan
Ann Arbor, MI 48109, USA
Prof. D. Hoelzle
Department of Mechanical and Aerospace Engineering
The Ohio State University
Columbus, OH 43210, USA
The ORCID identification number(s) for the author(s) of this article can be found under https://doi.org/10.1002/admt.202000386.

DOI: 10.1002/admt.202000386

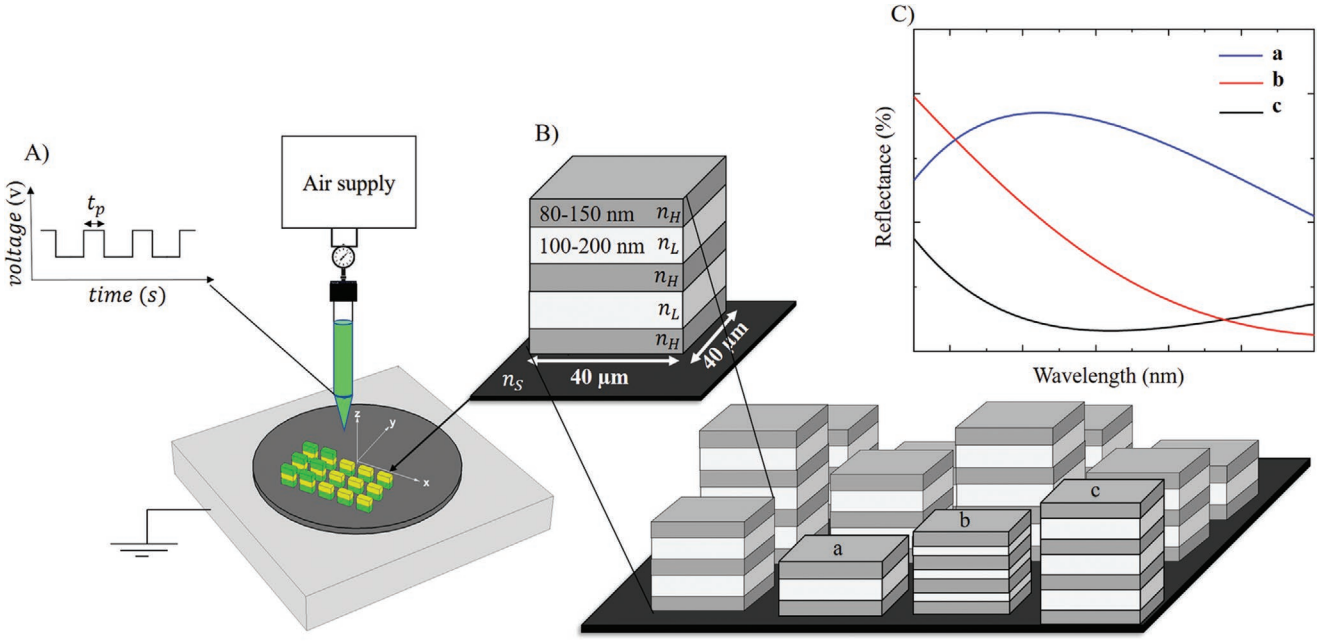

Figure 1. Multi-material thin-film fabrication by e-jet printing. A) Schematic of e-jet printing process. A high voltage pulse is applied to the nozzle to eject a droplet of material with droplet volume related to pulse-width, t_p. B) One-dimensional photonic crystals (1DPCs) to be fabricated by e-jet printing. n_L and n_H are low and high refractive indices of the corresponding polymeric materials. C) Reflectance response of a 1DPC can be tuned by modulating the number of layers and corresponding thicknesses.

flexibility in the classes of materials deposited, from biological materials to polymers and conductive inks.[20–22] Manufacturing speed can also be increased by integrating multiple parallel printheads depositing multiple materials onto one platform.[23]

The main elements of an e-jet printer (see schematic in **Figure 1**A) include a conductive nozzle holding the build material, conductive substrate, and voltage amplifier. We use a previously developed customized e-jet printer[24] with two printheads. An electric field is created by applying a voltage difference between the nozzle tip and the grounded substrate, changing the meniscus profile from a pendant shape to a cone shape, defined as a Taylor cone jet.[20] As the field strength increases, electrostatic forces overcome ink capillary tension and the liquid build material jets from the tip of the cone to the substrate.[21] The applied voltage can be pulsed with a pulse-width, t_p, from low voltage, V_l, to high voltages, V_h, as described in Figure 1A. Custom structures can be fabricated by synchronizing the stage motion with the voltage pulses, which enables a drop-on-demand printing mode with the ability to deposit sessile droplets at specified locations. It should be noted that a continuous jet-printing mode can also be used to deposit material on the substrate similar to line printing in ref. [25]. However, the fabrication of uniform thin films (film spatial resolution < 100 × 100 µm, film thickness < 100 nm) requires the deposition of high-resolution droplets (droplet diameter < 2 µm, droplet height < 100 nm). In a continuous jet-printing mode, high-resolution droplets are generated by increasing the applied voltage, which simultaneously results in higher frequency jetting. High stage speed is then required to space out the printed material on the substrate to form sessile droplets rather than large conglomerations of printed droplets. As the stage speed increases, additional dynamics and noise are introduced into the process, thus reducing the overall quality of the printed patterns. Thus, drop-on-demand printing offers more stability at a particular spatial resolution by controlling the release of a small volume of material at a desired coordinate and at a desired time.

Many applications require multi-material, layered structures with well-defined areas, smooth interfaces between layers, and controllable thicknesses; however, a systematic method to achieve these structures by e-jet is lacking. E-jet employs a complex ejection mechanism that is affected by the fluidic properties of the build material (e.g., surface tension, electrical conductivity, viscosity, density, etc.) and process parameters (e.g., nozzle size, electric field, the surface energy of the substrate, etc.). There are many challenges in material ejection and spreading that need to be investigated to understand the printing process and material interactions at the micro and nanoscale toward realizing the full potential of the e-jet printing process.

In Part I of this companion set, an empirical model is developed that correlates process parameters with material properties in multi-material, multi-layer structures with control of thickness at the nanoscale, and control of in-plane patterning at the microscale. First, we study the deposition of individual droplets and how they merge to form continuous layers. Second, we extend this result to multiple stacked layers comprising different materials, enabling structures like the vertical Bragg reflectors in Figure 1B. The reflectance of a Bragg reflector can be tuned by the number of layers and corresponding thicknesses (see Figure 1C). We outline process parameters that determine the quality of film formation, which in turn influences device functionality. We also highlight the

material properties and their scale-dependence that contribute to high-quality film formation.

A series of experiments are conducted to find a set of compatible materials that demonstrate stable jetting behavior during deposition as well as merging characteristics after the material has reached the substrate. Stable jetting behavior describes materials that form a stable, single Taylor cone jet[20] at the meniscus without clogging or evaporating. Good merging characteristics describes build materials that spread to a uniform thin-film on existing topography. In Part II of these companion manuscripts, a photonic crystal is fabricated using e-jet printing, with alternating layers of low and high refractive indices of commercially available photopolymers.[34] Design criteria are developed to select material combinations with favorable optical properties for the fabrication of a multi-material, multi-layer photonic crystal. The photonic responses of the structures printed in this work are quantified via a custom-developed microspectroscope.

Thin-film fabrication, using drop-on-demand e-jet printing, is a result of droplet ejection, droplet spreading, and droplet coalescence. Materials with stable jetting behavior will form a single stable Taylor cone jet[20] at the meniscus. After the material is ejected from the nozzle tip, a sessile droplet is formed on the substrate with a spherical cap shape that is defined based on the droplet diameter and contact angle.[26] The droplet geometry depends on the electric field, the kinetic energy imparted on the droplet at ejection, the surface tension of the droplet, surface energy of the substrate, rheological properties of the ink, and the viscous energy lost during spreading. Several previous studies on e-jet behavior have utilized UV-curable photopolymer inks deposited onto conductive, smooth silicon wafers as a model system. They are chosen here again for their combination of fluid properties as well as having the ability to be cured in situ, without requiring high temperature operations. As an example, NOA170 was chosen to investigate the formation of thin-films on a polished silicon substrate based on varying process parameters.

The controllable process parameters that can affect the applied electric field, and subsequent droplet volume, include: high voltage value, low voltage value, pulse-width (t_p), nozzle size, and standoff height (distance between the nozzle tip and the substrate). In this work, we intentionally adjust the droplet volume of a specific material using t_p, while keeping all other process parameters constant. We chose t_p because it has a direct mapping to droplet volume[27] and reduces the introduction of additional jetting dynamics and disturbances, such as nozzle arcing, which are more likely to occur with changes in other process parameters like high voltage or standoff height. By design, each droplet is a result of a single droplet released within the designated t_p. Successive droplets can be placed at a certain distance (center to center) from each other, defined as pitch, to form a film. The average thickness of a film, $\overline{g}$, and the root mean square (RMS) surface roughness, s_q, are defined as:

$$\overline{g} = \frac{1}{N_1 \times N_2} \sum_{i=1}^{N_1} \sum_{j=1}^{N_2} g_{i,j} \tag{1}$$

$$s_q = \frac{1}{N_1 \times N_2} \sqrt{\sum_{i=1}^{N_1} \sum_{j=1}^{N_2} \left(\overline{g} - g_{i,j}\right)^2} \tag{2}$$

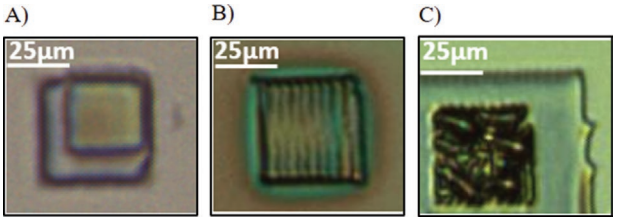

Figure 2. Material interactions at the microscale. A) Fully merged: Loctite3526 fully merges on NOA170 with thickness and RMS roughness of 90 and 6 nm, respectively. B) Partially merged: NOA170 partially merges on NOA144 with thickness and RMS roughness 175 and 40 nm, respectively. C) Unmerged: NOA170 does not merge on NOA1348 with thickness and RMS roughness 250 and 200 nm, respectively.

where $g_{i,j}$ is the topography of the pattern at the discretized coordinate of (i,j), and N_1 and N_2 are the total number of discretized coordinates in the X and Y direction. Note that both $\overline{g}$ and s_q are measured using an integrated AFM.

Roughness is a representation of the merging quality of a film such that a low s_q value indicates a smoother film. The thickness and roughness of the printed films can be regulated by adjusting the droplet volume and pitch. As such, pitch and t_p are independent variables while film thickness and roughness are dependent variables. At small t_p or large pitch values (pitch >> D), the droplets become smaller than the pitch, which yields voids in the pattern and increases the film's roughness. To quantify film quality, we define a thin-film pattern with a thickness smaller than 200 nm as fully merged if it has an s_q value less than 20 nm, partially merged for s_q values between 20 and 50 nm, and unmerged for s_q values greater than 50 nm. **Figure 2** shows these interactions at the microscale.

Figure 3A shows the effect of t_p on the average thickness and corresponding RMS surface roughness (represented as error bars) of NOA170 films (60 × 60 µm). The controlled process parameters include: V_h = 500 V, V_l = 250 V, nozzle size = 1 µm, standoff height = 20 µm, and pitch = 2.4 µm. The pulse width, t_p, is varied between 0.5 and 12 ms to investigate its effect on film quality. Note that the diameter of a droplet is varied by changing t_p. It is observed that decreasing t_p from 12 to 2 ms decreases the pattern thickness and roughness. A pulse-width of 1 ms (t_p = 1 ms) resulted in the lowest roughness (s_q = 7.23 nm) with a film thickness of 95 nm.

The influence of pitch on average thickness and roughness of NOA170 films is presented in Figure 3B. We use a raster type motion to print a continuous line that merges to form films, as presented in the inset of Figure 3B. The controlled process parameters are the same as those used to evaluate the effect of pulse width; however, we set t_p to be 1 ms, which yields an average droplet diameter of D = 2.83 ± 0.12 µm, and vary the pitch between 1 and 2.9 µm. As the pitch increases, both the roughness and thickness decrease. A pitch of 2.5 µm resulted in the lowest roughness (s_q = 8.41 nm) with an average thickness of 89.63 nm.

These results suggest that the thin-film fabrication process has two parameter selection steps: (1) eject controlled droplets by pulsing from low to high voltage over a designed time period (shorter t_p leads to smaller droplets), and (2) adjust the pitch between deposited droplets to achieve thin, uniform patterns (pitch values ≈ droplet diameter D).

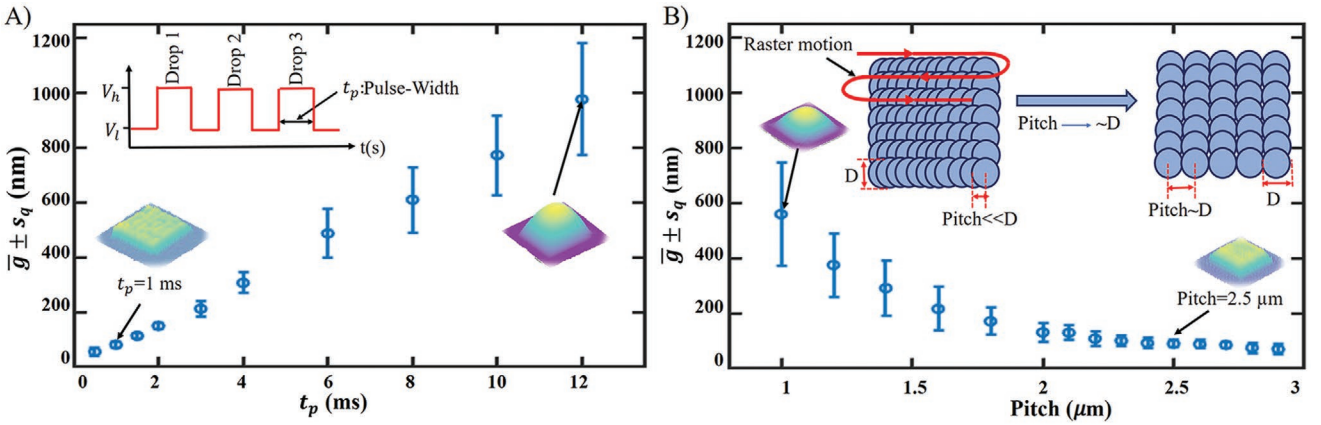

Figure 3. Effect of process parameters on average thickness ($\bar{g}$) and surface roughness (s_q) of NOA170 films. Error bars indicate RMS roughness measured by an integrated AFM. Patterns are printed on bare silicon using drop-on-demand e-jet printing in a raster motion. A) Effect of pulse-width (t_p) on pattern thickness and roughness for a fixed pitch = 2.4 μm. B) Effect of pitch on pattern thickness and roughness for a fixed t_p = 1 ms (droplet diameter of $D = 2.83 \pm 0.12$ μm). Convex patterns result for pitch $\ll D$, uniform patterns result for pitch $\approx D$, and rough patterns result for pitch $> D$.

In the previous section, process parameters governing the deposition of smooth, nanoscale films onto a uniform surface (e.g., polished silicon) were investigated. However, in some cases, tuning the process parameters does not guarantee a fully merged film. It is possible for a build material to merge into a uniform film on one material, but not on a different material. This raises the question of how to determine appropriate material interactions in multi-material structures that are fabricated in a layer-by-layer fashion. For example, to create a multi-material structure such as a photonic crystal in Figure 1B, a refractive index contrast ($\Delta n = n_H - n_L$) must be achieved between neighboring layers, which introduces variations in surface energy for each additional layer being deposited. To quantify the impact of these variations, we study the shape of sessile droplets of a build material on a previous surface. A range of photopolymers are investigated: NOA170, Loctite3526, NOA144, NOA142, NOA13825, NOA138, NOA13775, NOA1369, and NOA1348, with refractive indices ranging from n = 1.35–1.71, which provides an index contrast maximum of $\Delta n = 0.35$. We chose NOA170 as the n_H material due to its high refractive index, $n_H = 1.70$, and search for a low refractive index material (n_L) to fabricate a multi-layer structure such as Figure 1B. Moving forward, we will refer to the silicon wafer as the primary substrate, while previously deposited, fully merged and cured photopolymer surfaces (Figure 2) will be referred to as secondary substrates.

The substrate-ink interaction can be defined by the contact angle, which is a function of fluidic properties of the build material (liquid surface tension (LST), viscosity, evaporation rate, density, etc.), and surface energy of the previous layer. Several previous studies have investigated how tuning the solid surface energy (SSE) of a substrate can affect droplet shape and subsequent feature resolution in inkjet printing.[25,27] This has been extended to high-resolution e-jet printing, where the microscale contact angles of droplets were used to predict the merging quality of lines[28] on varying SSE surfaces. Microscale contact angles (droplets of 2–10 μm) are also used here to predict the roughness of a deposited layer of a build material on the surface of a previously printed material. In addition, we explored if macroscale surface energetic measurements could be used to gain insights into material behavior at the microscale; however, no relationship was found. This highlights the fact that material interactions at the microscale are different from the macroscale, and subsequently previous theories derived for the macroscale are not sufficient to describe the layer-to-layer dynamics at the microscale. As such, we only focus on the microscale results, and contact angle measurements at the macroscale are presented in the Supporting Information.

The microscale material interactions in **Figure 4**A include: NOA170 printed on the primary substrate (Figure 1B, layer 1), the n_L materials printed on top of a secondary substrate of NOA170 (unfilled markers in Figure 4A and layer 2 in Figure 1B), and NOA170 printed on secondary substrates of n_L photopolymers (filled markers in Figure 4A and layer 3 in Figure 1B). The low refractive index materials in this work include: Loctite3526, NOA144, NOA142, NOA13825, NOA138, NOA13775, NOA1369, and NOA1348. Three regimes defined by the roughness of the formed film (60 × 60 μm) of a build material on a substrate are delineated for ease of characterization. A monotonically increasing linear relationship on a log–log plot is found between the contact angle of a single droplet (2–10 μm) of a build material on a substrate (primary/secondary of a different material) and the roughness of a printed film of the same build material on the substrate. It is observed that build materials with a low contact angle have a higher likelihood of adhering to previous surfaces and forming a uniform thin-film on them. Focusing on the microscale measurements in Figure 4A, a printed layer of NOA170 serves as the secondary substrate for the deposition of low index materials. All low index inks exhibit fully merged thin-films (<200 nm) with low contact angles (<15°) and low RMS surface roughness (<10 nm). Interestingly, the deposition of NOA170 on top of low refractive index materials (layer 3) does not perform as smoothly. Depending on the material in the previous layer, the contact angles range from 10° to 50° with resultant pattern roughness values ranging from less than 20 nm to greater than 200 nm. The only low index material that NOA170 fully merges onto is filtered Loctite3526, while NOA170 printed onto several other low index ink secondary substrates shows partial merging.

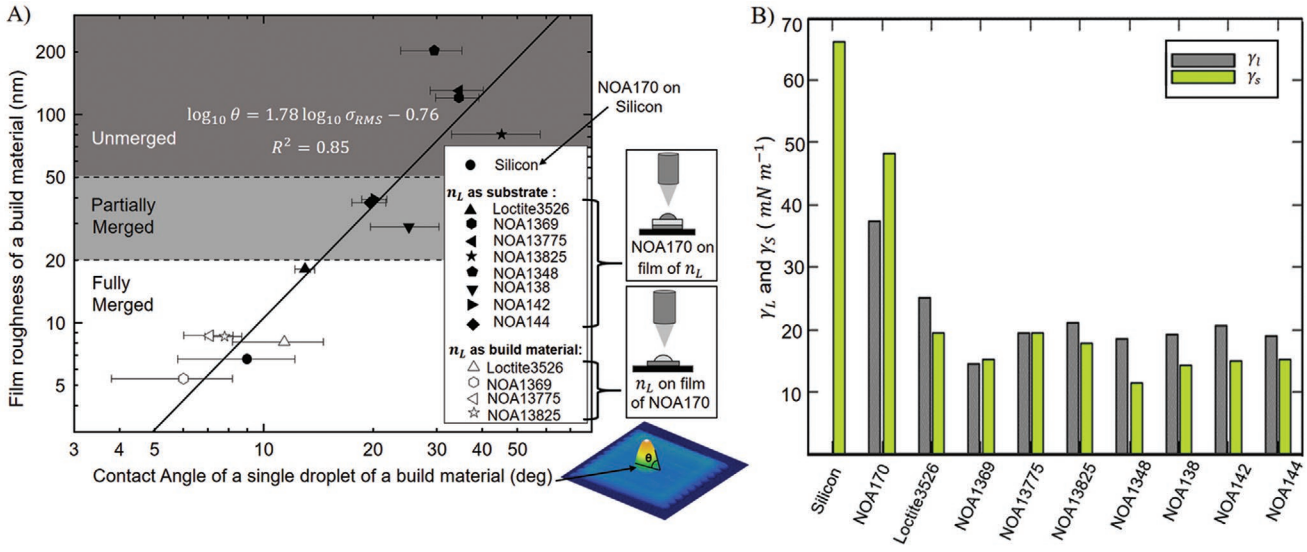

Figure 4. Surface energetic investigation to determine wetting behavior of inks on previous substrates. A) Contact angle measurements of a single droplet (2–10 µm) versus RMS roughness of a film (60 × 60 µm) of the same build material onto a primary or secondary substrate. 3D view of an AFM scan of a single droplet of a build material on a secondary substrate is shown near the horizontal axis. Filled markers describe interactions of NOA170 on n_L materials, while unfilled markers represent n_L materials on NOA170 films. Results indicate: full merging for $\theta < 15°$, partial merging for $15° < \theta < 25°$, and failure to merge for $\theta > 25°$. Further details are provided in Tables S3 and S4 (Supporting Information). B) Solid surface energy and liquid surface tension of all inks in this work.

It should be mentioned that the results in Figures 4A describe material spreading on a uniform surface with low roughness (<10 nm). Previous work has demonstrated the impact of previous layer roughness on material spreading.[29] Our investigations in this work suggest that at the microscale, in addition to the topology, chemical heterogeneity of the previous layer may play a role in surface roughness (Figure S2A, Supporting Information). Future studies will explore the relationship between thickness of the current layer and roughness of the previous layer.

The effects of process parameters demonstrated in Figure 3, combined with the empirical model determined from Figure 4A, provide the first steps toward the development of a generalized model for describing material spreading of printed layers of polymers as a function of process parameters and the contact angle of printed single droplets. Additional material interactions should be explored along with a parameterization of different material properties such as density, viscosity, and conductivity to derive a normalized model that can be used to predict material spreading for a broad range of materials at the microscale.

To further explore material spreading, a macroscale surface energetics study is undertaken using the standard method of Owens and Wendt[30] and Wu.[31] While this work focuses on controlling material behaviors at the microscale, measuring SSE at these length scales is quite difficult; thus, requiring a surface energetics study at the macroscale. The results of this study are summarized in Figure 4B. The silicon wafer showed the highest average SSE (γ_s = 66.3 mN m^{-1}), followed by NOA170 (γ_s = 48.3 mN m^{-1}), while the lower index materials (n_L = 1.35–1.51) exhibited significantly lower SSE values (γ_s = 11.5–19.5 mN m^{-1}). From previous reports,[25] it is expected that a material with a high SSE value will be a more favorable substrate for realizing uniform film formation of the next layer. This supports our observations that NOA170 is a favorable substrate for the low index materials evaluated here.

The LST values of all inks are evaluated using the pendant droplet method.[32] In this paper, a highly cohesive ink is defined as an ink that has a high LST value and exhibits poor wetting behavior due to a preference for attaching to itself rather than adhering to a substrate. On the other hand, poorly cohesive inks (low LST values) are not able to remain bonded to themselves to form a uniform pattern on existing topographies. Based on the values provided in Figure 4B, NOA170 has a relatively high LST value (37.3 mN m^{-1}). Note that NOA170 will spread readily on a silicon substrate (γ_s (silicon) > γ_l (NOA170)), but exhibits mixed merging behavior on lower SSE valued surfaces. We observed that a highly cohesive ink (e.g., NOA170) is unlikely to adhere to a low surface energy substrate (γ_l (NOA170) > γ_s (n_L materials)). Through our studies we identified two approaches for managing these interactions. First, the SSE value of a merged layer of an n_L material could be increased using in situ modifications, such as atmospheric plasma treatments.[33] Second, efforts may be spent in determining methods for decreasing the LST of a high index material (NOA170 in this case) to promote improved merging quality.

From these studies, we have concluded that material interactions at the microscale are a result of a trade-off between contact angle, SSE, and LST values. For example, printed droplets of NOA170 on NOA1348 and NOA138 secondary substrates exhibit similar contact angles at the microscale (Figure 4A). However, a lower SSE value for NOA1348 may help explain why NOA170 fails to result in a merged film on this surface. We also note that the filtered Loctite3526 and NOA13775 have similar SSE values; however, the higher contact angle of printed droplets of NOA170 on the printed NOA13775 surface results in a

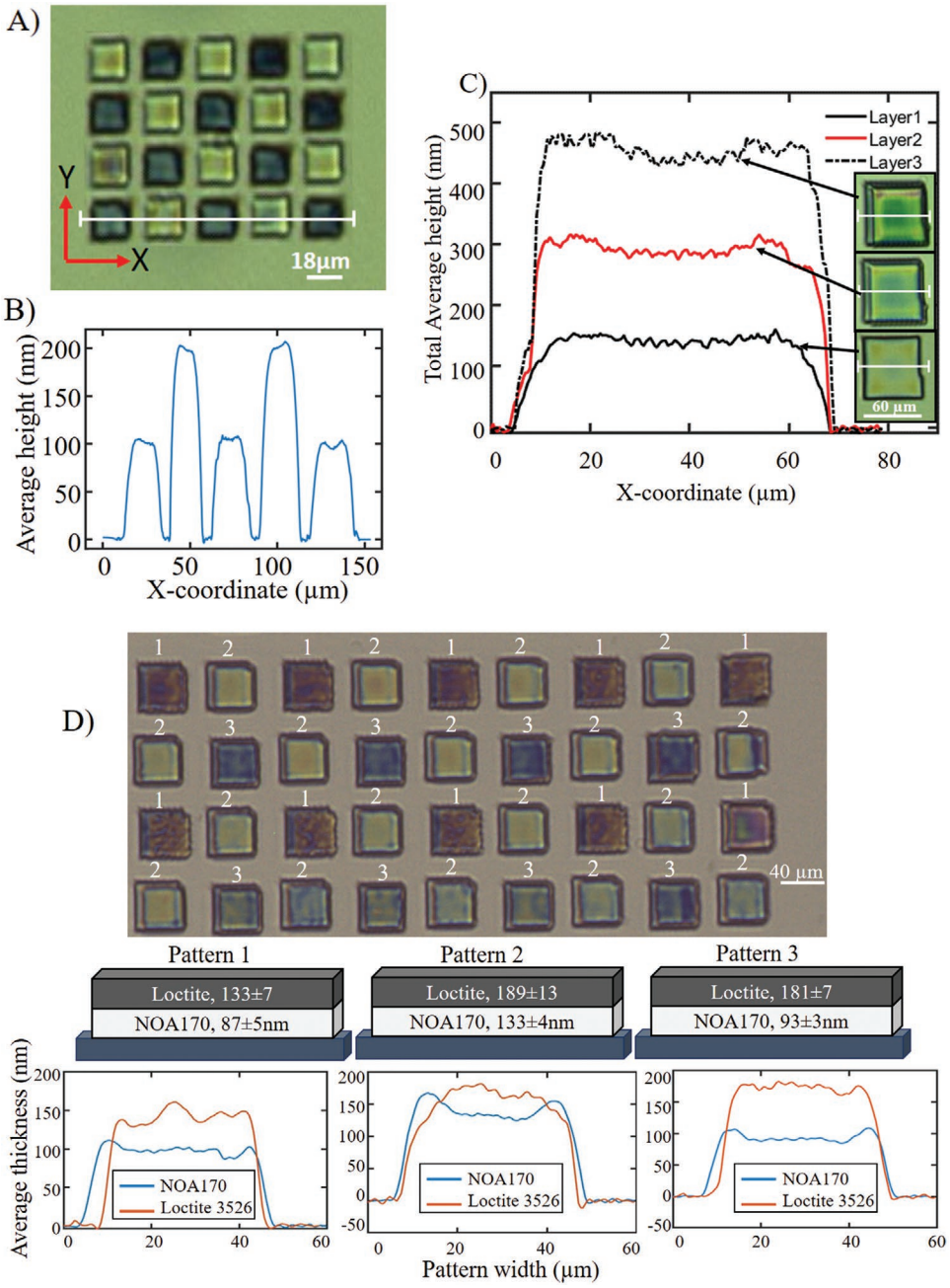

Figure 5. Multi-material thin-film fabrication using drop-on-demand of e-jet printing. A) Multi-material, single layer fabrication of high-resolution thin-film patterns using e-jet printing. The white line shows the height average across five pixels in the Y direction. The lighter color patterns are NOA13825 with thickness and roughness of 205 and 12 nm, respectively, and the darker color patterns are NOA170 with thickness and roughness of 101 and 5 nm. B) Average pattern height across five pixels through the center of the last row. C) Multi-material and multi-layer fabrication using e-jet printing. D) Multi-material and multi-layer e-jet printed Bayer array filter.

rougher surface deposition for films of NOA170. In addition, partial merging was observed with the deposition of NOA170 on NOA138, NOA142, and NOA144; which also showed moderate contact angles of printed NOA170 droplets ($15° < \theta < 25°$) as compared to NOA1369 with similar SSE values.

This section provides a demonstration of e-jet printing of multi-layer thin-film structures. The results presented in the previous sections were used to select appropriate ink combinations. The experimental results in this section were heuristically obtained by determining appropriate process parameters that would yield the desired film thicknesses. The desired thickness values were derived from simulation results provided in our companion paper[34] and chosen as values that would provide a specific optical outcome.

Figure 5A shows multi-material microstructures that were fabricated by e-jet printing of two high viscosity adhesives

at room temperature. The design goal is to deposit uniform high-resolution NOA170 and NOA13825 patterns with layers of 100 nm and 200 nm average thickness, respectively. The darker color patterns were 20 × 20 μm films of NOA170 (4400–5000 cP) with an average thickness and RMS roughness of 101 and 5 nm, respectively. The lighter colors were deposited 17 × 17 μm films of NOA13825 (5600 cP) with an average thickness and RMS roughness of 205 and 12 nm, respectively. The distance between the patterns was set at 5 μm. The pattern profile across the last row of the printed structure (shown in Figure 5B) highlights the flexibility and repeatability of the e-jet printing process.

The multi-material, multi-layer fabrication of two high viscosity materials using e-jet printing is presented in Figure 5C: NOA170 was printed in layers 1 and 3, while filtered Loctite3526 was printed in layer 2. To achieve the desired effect, each layer is designed to be approximately 160 nm thick. The e-jet process parameters for NOA170 were V_h = 600 V, V_l = 200 V, t_p = 1 ms, f = 20 Hz, and pitch = 1.8 μm. The e-jet process parameters for Loctite3526 were V_h = 500 V, V_l = 250 V, t_p = 5 ms, f = 20 Hz, and pitch = 2 μm. At each layer, the liquid patterns were UV-cured and their topography was measured using the integrated AFM. Figure 5C shows the corresponding average total height map over five pixels from the middle of the pattern at each layer. The overall variation (roughness/total height) in the total stack height was less than 6% across a single layer and 4% across the entire stack. The average total height is 159 ± 9 nm for layer 1, 325 ± 13 nm for layer 2, and 489 ± 17 nm for layer 3, respectively. The maximum RMS roughness in all layers is less than 17 nm, which is a demonstration of the flatness in the overall height. The integration of control to the e-jet process could be used to mitigate height variations.

Figure 5D presents a high-resolution e-jet printed Bayer filter array using a high refractive index polymer (NOA170, n = 1.7) and a medium refractive index material (Loctite3526, n = 1.51). Patterns 1, 2, and 3 are associated with the red, blue, and green color spectrum, respectively, and are equally spaced with a 15 μm offset with roughness smaller than 13 nm. One goal in creating these bi-layer samples was to show the e-jet process could independently control layer thickness, regardless of the previous printed layer thickness, with the end result being control over the reflected light intensity at specific areas of the spectrum. Thus, the following layer goals were set with the first and second layers at 90 and 130 nm for pattern 1, 130 and 180 nm for pattern 2, and 90 and 180 nm for pattern 3, respectively. These combinations achieved red, green, and blue reflected peak intensity with differing combinations of thickness of both the NOA170 as base layer and Loctite3526 as the second layer. The optical response of these structures is explored further in ref. [34]. Through drop-on-demand e-jet printing, we controlled the thickness of each layer precisely and by design. As demonstrated, it is possible to create a variable color spectrum using e-jet printing, as the color spectrum is correlated with the layer thickness and the corresponding refractive indices of each layer.[35] Therefore, for a fixed material combination, the optical properties can be varied by adjusting the layer thickness.

The experimental results in this section show that the thickness variation is within 6% across a single layer. Different factors affect these variations: (1) The integrated Nanite AFM has ±10 nm thermal noise that directly affects the roughness measured. (2) Commercial inks may contain large particles that increase thickness variations. (3) E-jet is an iteration varying process and different factors such as nozzle clogging, environment temperature and humidity, and more can affect the deposition process and eventually affect the roughness. Future work will explore the integration of control strategies to minimize variations and achieve higher fidelity printed patterns.

In this work, we presented an empirical model for e-jet printing that influences the merging quality of UV-curable polymers in thin-film, multi-material, layered microstructures. A set of material criteria were introduced that are required for material ejection as well as material merging in e-jet printing. The experimental results highlighted the potential of e-jet printing as a substitute for other manufacturing techniques, such as lithography, to fabricate high-resolution devices that are made of multiple thin layers of different materials. Furthermore, it was experimentally demonstrated that at the microscale, high-quality films were most probable with the following material combinations (1) low contact angle, (2) high surface tension of the build material, and (3) high surface energy of the previous layer. Ultimately, the controllability and repeatability of e-jet printing were demonstrated by fabricating a Bayer filter that consisted of different colors across the spectrum using drop-on-demand printing.

Experimental Section

Material Preparation: Several optical adhesives (Norland Optical Products (NOA)) as well as a commercial Loctite formulation were used. For high-resolution patterning, nozzles smaller than 1 μm in inner diameter were used with a 20 μm standoff height. Some inks contained large particles (e.g., comprising resin, a long chain oligomer, or foreign moieties) that must be filtered in order to reduce the chance of nozzle clogging. Before running the experiments, Loctite3526 using high pressure and a filter with 0.22 μm diameter pores were filtered. The removal of large particles had the added benefit of reducing the surface roughness of the printed patterns. However, it was noted that filtering in some cases changed other ink properties, e.g., filtered NOA170 had a smaller refractive index value than unfiltered NOA170, while also exhibiting an unstable spray jet[36] instead of a single stable jet mode at the same standoff height and voltage.

Contact Angle Measurement: To measure contact angles at the microscale, an array of droplets of a build material was deposited onto a surface (primary or secondary substrate of another material). The droplets were cured, and their topographies were measured using an integrated Nanite AFM (inset of the horizontal axis in Figure 4A). It was assumed that the contact angle of a droplet did not change with UV-curing; this assumption was confirmed using a slightly larger droplet (>20 μm) and an integrated camera. The raw AFM data were then post-processed in the software package "Gwyddion" to measure the topography and the corresponding contact angles. Fifteen droplets were deposited with varying t_p to generate droplets with diameters ranging from 2 to 10 μm. These droplets were used to measure the average contact angle and corresponding standard deviations. The standard deviation of the printed droplets was low (<6°, except for NOA13825 that exhibited clogging issue) as shown in Figure 4A. This indicated that the contact angle at the microscale did not depend on the droplet diameter. At the macroscale, contact angle measurements were conducted on a Ramé-Hart goniometer by placing millimeter-scale droplets of various inks on the respective surfaces. "DROPImage" software was used to fit a curve to the acquired image of the droplet and measure the contact angle. This is shown in Figure S3B (Supporting Information).

Liquid Surface Tension Characterization: The LST values of all inks were determined using the pendant droplet method. Based on the density of the ink and the resulting droplet shape underneath a nozzle, it was possible to compute the LST of an ink. This study was also carried out on a Ramé-Hart goniometer. Density measurements were conducted by weighing a known volume of each ink. A summary of density measurements and resulting LST measurements is given in Table S1 (Supporting Information).

Solid Surface Energy Characterization: All of the photopolymers studied in this work were spin-coated onto silicon wafers (≈2 × 2 cm) at 6000 RPM within an inert glove box and cured under 365 nm light for 15 min to ensure a full cure. The contact angle-based methods of Owens–Wendt and Wu were selected for this study to estimate the SSE value.[27,28] Three droplets of two different probe liquids, deionized water (γ_l = 72.8 mN m^{-1}) and diiodomethane (50.8 mN m^{-1}), were placed at three different positions on the spin-coated samples (as well as the silicon substrate), and the contact angles were measured using a Ramé-Hart goniometer. The SSE values of all inks studied in this work are given in Table S2 (Supporting Information).

It should be mentioned that material deposition had been done in an ambient atmosphere. However, the patterns were cured in a nitrogen atmosphere due to oxygen inhibition of the photopolymerization of the inks (excluding Loctite 3526). This was achieved by creating an enclosure around the LED curing bulb and flowing nitrogen at a high rate over the surface. The surface energies were not measured in an inert atmosphere. The macroscale surface energetics were determined at room temperature and pressure.

Supporting Information

Supporting Information is available from the Wiley Online Library or from the author.

Acknowledgements

Reference [34] was updated on September 28, 2020, after initial publication online. The authors would like to acknowledge Steve Morris, Erin Evke, and Chris Pannier for helpful conversations and the Tuteja Research Lab at the University of Michigan for support and guidance on completing the surface energetics studies. This work was supported by the National Science Foundation (CMMI 1727894).

Conflict of Interest

The authors declare no conflict of interest.

Keywords

additive manufacturing, contact angle, multi-material structures, surface energy, thin-film fabrication

Received: April 22, 2020
Revised: July 10, 2020
Published online: August 16, 2020

[1] M. E. Calvo, H. Míguez, *Chem. Mater.* **2010**, *22*, 3909.
[2] X. Zhu, Q. Xu, H. Li, M. Liu, Z. Li, K. Yang, J. Zhao, L. Qian, Z. Peng, G. Zhang, J. Yang, F. Wang, D. Li, H. Lan, *Adv. Mater.* **2019**, *31*, 1902479.
[3] X. Zhu, Z. Li, Y. Hu, H. Li, J. Yang, H. Lan, *Opt. Laser Technol.* **2020**, *123*, 105943.
[4] J. B. Szczech, C. M. Megaridis, D. R. Gamota, J. Zhang, *IEEE Trans. Electron. Packag. Manuf.* **2002**, *25*, 26.
[5] N. Duraisamy, N. M. Muhammad, H.-C. Kim, J.-D. Jo, K.-H. Choi, *Thin Solid Films* **2012**, *520*, 5070.
[6] Y. Wu, H. Shen, S. Ye, D. Yao, W. Liu, J. Zhang, K. Zhang, B. Yang, *ACS Appl. Mater. Interfaces* **2016**, *8*, 28844.
[7] M. Karl, J. M. E. Glackin, M. Schubert, N. M. Kronenberg, G. A. Turnbull, I. D. W. Samuel, M. C. Gather, *Nat. Commun.* **2018**, *9*, 1525.
[8] P. C. Chang, J. Lee, D. Huang, V. Subramanian, A. R. Murphy, J. M. J. Fréchet, *Chem. Mater.* **2004**, *16*, 4783.
[9] H. Sirringhaus, T. Kawase, R. H. Friend, T. Shimoda, M. Inbasekaran, W. Wu, E. P. Woo, *Science* **2000**, *290*, 2123.
[10] G. Manfredi, P. Lova, F. Di Stasio, P. Rastogi, R. Krahne, D. Comoretto, *RSC Adv.* **2018**, *8*, 13026.
[11] F. Ferrarese Lupi, T. J. Giammaria, F. G. Volpe, F. Lotto, G. Seguini, B. Pivac, M. Laus, M. Perego, *ACS Appl. Mater. Interfaces* **2014**, *6*, 21389.
[12] C. O. Ramírez Quiroz, C. Bronnbauer, I. Levchuk, Y. Hou, C. J. Brabec, K. Forberich, *ACS Nano* **2016**, *10*, 5104.
[13] N. Anderson, P. Prabhat, T. Erdogan, in *Multiphoton Microscopy in the Biomedical Sciences XII*, **2012**, p. 82260O.
[14] J. Wang, L. Wang, Y. Song, L. Jiang, *J. Mater. Chem. C* **2013**, *1*, 6048.
[15] J. Jang, H. Kang, H. C. N. Chakravarthula, V. Subramanian, *Adv. Electron. Mater.* **2015**, *1*, 1500086.
[16] A. G. Kelly, T. Hallam, C. Backes, A. Harvey, A. S. Esmaeily, I. Godwin, J. Coelho, V. Nicolosi, J. Lauth, A. Kulkarni, S. Kinge, L. D. A. Siebbeles, G. S. Duesberg, J. N. Coleman, *Science* **2017**, *356*, 69.
[17] H. Minemawari, T. Yamada, H. Matsui, J. Tsutsumi, S. Haas, R. Chiba, R. Kumai, T. Hasegawa, *Nature* **2011**, *475*, 364.
[18] A. Camposeo, L. Persano, M. Farsari, D. Pisignano, *Adv. Opt. Mater.* **2019**, *7*, 1800419.
[19] S. D. Hoath, *Fundamentals of Inkjet Printing: The Science of Inkjet and Droplets*, John Wiley & Sons, Weinheim **2016**.
[20] J.-U. Park, M. Hardy, S. J. Kang, K. Barton, K. Adair, D. K. Mukhopadhyay, C. Y. Lee, M. S. Strano, A. G. Alleyne, J. G. Georgiadis, P. M. Ferreira, J. A. Rogers, *Nat. Mater.* **2007**, *6*, 782.
[21] M. S. Onses, E. Sutanto, P. M. Ferreira, A. G. Alleyne, J. A. Rogers, *Small* **2015**, *11*, 4237.
[22] Y. Han, J. Dong, *J. Micro Nano-Manuf.* **2018**, *6*, 40802.
[23] E. Sutanto, K. Shigeta, Y. K. Kim, P. G. Graf, D. J. Hoelzle, K. L. Barton, A. G. Alleyne, P. M. Ferreira, J. A. Rogers, *J. Micromech. Microeng.* **2012**, *22*, 045008.
[24] C. Pannier, L. Ojeda, Z. Wang, D. Hoelzle, K. Barton, *Mechatronics* **2018**, *56*, 268.
[25] S. Schlisske, M. Held, T. Rödlmeier, S. Menghi, K. Fuchs, M. Ruscello, A. J. Morfa, U. Lemmer, G. Hernandez-Sosa, *Langmuir* **2018**, *34*, 5964.
[26] C. P. Pannier, K. Barton, D. Hoelzle, Z. Wang, in *ASME 2015 Dyn. Syst. Control Conf.*, **2016**.
[27] S. H. Lee, Y. J. Cho, *J. Electr. Eng. Technol.* **2012**, *7*, 91.
[28] J. Park, B. Kim, S.-Y. Kim, J. Hwang, *Appl. Phys. A* **2014**, *117*, 2225.
[29] C. Pannier, M. Wu, D. Hoelzle, K. Barton, in *2019 Amer. Control Conf.*, IEEE, Philadelphia, PA **2019**.
[30] D. K. Owens, R. C. Wendt, *J. Appl. Polym. Sci.* **1969**, *13*, 1741.
[31] S. Wu, *J. Polym. Sci., Part C: Polym. Symp.* **1971**, *34*, 19.
[32] S. M. I. Saad, Z. Policova, A. W. Neumann, *Colloids Surf. A Physicochem. Eng. Asp.* **2011**, *384*, 442.
[33] E. R. Ionita, M. D. Ionita, E. C. Stancu, M. Teodorescu, G. Dinescu, *Appl. Surf. Sci.* **2009**, *255*, 5448.
[34] B. Iezzi, Z. Afkhami, S. Sanvordenker, D. Hoelzle, K. Barton, M. Shtein, *Adv. Mater. Technol.* **2020**, *5*, 2000431.
[35] P. Lova, G. Manfredi, D. Comoretto, *Adv. Opt. Mater.* **2018**, *6*, 1800730.
[36] M. Cloupeau, B. Prunet-Foch, *J. Aerosol Sci.* **1994**, *25*, 1021.